Experimental Study of the Ion Critical-Gradient Length and Stiffness Level and the Impact of Rotation in the JET Tokamak

P. Mantica,[1] D. Strintzi,[2] T. Tala,[3] C. Giroud,[4] T. Johnson,[5] H. Leggate,[4] E. Lerche,[6] T. Loarer,[7] A. G. Peeters,[8] A. Salmi,[9] S. Sharapov,[4] D. Van Eester,[6] P. C. de Vries,[4] L. Zabeo,[4] and K.-D. Zastrow[4]

[1]*Istituto di Fisica del Plasma "P. Caldirola," Associazione Euratom-ENEA-CNR, Milano, Italy*
[2]*National Technical University of Athens, Association Euratom Hellenic Republic, GR-15773 Athens, Greece*
[3]*Association EURATOM-Tekes, VTT, P.O. Box 1000, FIN-02044 VTT, Finland*
[4]*Culham Science Centre, EURATOM/UKAEA Association, OX14 3DB, Abingdon, United Kingdom*
[5]*Association EURATOM-VR, Fusion Plasma Physics, EES, KTH, Stockholm, Sweden*
[6]*LPP-ERM/KMS, Association Euratom-Belgian State, TEC, B-1000 Brussels, Belgium*
[7]*CEA Cadarache, Association EURATOM-CEA, 13108, St Paul-Lez-Durance, France*
[8]*Centre for Fusion Space and Astrophysics, University of Warwick, Coventry 7AL, United Kingdom*
[9]*Association EURATOM-Tekes, Helsinki University of Technology, P.O. Box 2200, FIN-02150 TKK, Finland*

(Received 12 October 2008; published 29 April 2009)

Experiments were carried out in the JET tokamak to determine the critical ion temperature inverse gradient length ($R/L_{\mathrm{Ti}} = R|\nabla T_i|/T_i$) for the onset of ion temperature gradient modes and the stiffness of T_i profiles with respect to deviations from the critical value. Threshold and stiffness have been compared with linear and nonlinear predictions of the gyrokinetic code GS2. Plasmas with higher values of toroidal rotation show a significant increase in R/L_{Ti}, which is found to be mainly due to a decrease of the stiffness level. This finding has implications on the extrapolation to future machines of present day results on the role of rotation on confinement.

DOI: 10.1103/PhysRevLett.102.175002 PACS numbers: 52.25.Fi, 52.35.Ra, 52.55.Fa

The anomalous character of ion heat transport in tokamaks, 1–2 orders of magnitude higher than collisional transport, is a long dated experimental observation. Recent studies are reported, e.g., in [1–4]. A comprehensive theoretical description of turbulent ion heat transport as driven by ion temperature gradients (ITG) modes has been developed and applied to physics based predictions of confinement in present and future devices [5–8]. ITGs feature a threshold in the inverse ion temperature gradient length ($R/L_{\mathrm{Ti}} = R|\nabla T_i|/T_i$, with R the tokamak major radius) above which the ion heat flux (q_i) increases strongly with R/L_{Ti}. This property leads to stiffness of T_i profiles with respect to changes in heating profiles. The level of stiffness characterizes how strongly T_i profiles are tied to the threshold. Experimental observations of the correlation between edge and core T_i values [2,9–11] and of an abrupt change of slope of the q_i vs R/L_{Ti} curve built using their radial excursion [1,3,4] support this theoretical picture. However, no dedicated experimental studies have yet been performed to build the q_i vs R/L_{Ti} curve at a given radius and keeping all parameters unchanged, which is the correct procedure to determine the local threshold and stiffness level. Recent T_i modulation experiments in JET [12] have provided the first measurements of the ion stiffness level by determining the slope of the q_i vs R/L_{Ti} curve around the modulation point. The validation of theoretical predictions for ion threshold and stiffness, their parametric dependences, and threshold upshifts due to rotational shear or nonlinear effects is of high relevance for the operation of future devices because the core T_i and fusion power achievable for a given T_i pedestal depend crucially on threshold and stiffness.

The JET tokamak ($R = 2.96$ m, $a = 1$ m) is equipped with a high quality active Charge Exchange Spectroscopy (CX) diagnostics for T_i and toroidal rotation (ω_t) measurements and a multifrequency Ion Cyclotron Resonance Heating (ICRH) system for flexible and fairly localized ion heating either using (H)-D or (^{3}He)-D minority schemes. These tools, together with JET's large size and low normalized ion gyroradius, make it an ideal device to perform on ions studies of threshold and stiffness as earlier performed on electrons [13–15]. This Letter describes first experiments in JET determining the ITG threshold and stiffness in low rotation plasmas, comparison with theory, and an experimental evaluation of the impact of rotation.

Experimentally, the identification of the ITG threshold and stiffness requires a scan of the core q_i at constant edge q_i, to keep edge properties constant, while maintaining reasonably unchanged other plasma parameters such as density, safety factor profile, T_e/T_i, Z_{eff}, rotation. Both electron and ion heat fluxes are predicted by theory to follow a gyro-Bohm scaling, at least for low values of the normalized gyroradius, so that q_i can be written in a general way as [16]

$$q_i = q_i^{\mathrm{res}} + n_i q^{1.5} \chi_s \frac{T_i^2 \rho_i}{eBR^2} \frac{R}{L_{T_i}} f\left[\frac{R}{L_{T_i}} - \frac{R}{L_{T_{i\mathrm{crit}}}}\right] \times H\left[\frac{R}{L_{\mathrm{Ti}}} - \frac{R}{L_{T_{i\mathrm{crit}}}}\right] \quad (1)$$

where q_i^{res} is the residual flux, including the neoclassical

flux, n_i the ion density, q the safety factor, B the magnetic field, e the electron charge, $\rho_i = (m_i T_i)^{1/2}/eB$, m_i the ion mass, and H the Heaviside function. From the curve of the gyro-Bohm normalized flux q_i^{norm} vs R/L_{Ti}, the threshold $R/L_{\mathrm{Ti\,crit}}$ can be identified as the intercept at neoclassical flux and the stiffness level χ_s can be inferred from the slope. This implies a normalization of q_i over a factor $n_i q^{1.5} T_i^{5/2}/R^2 B^2$. In the following, n_e was used as an estimator for n_i, since the plasmas have similar impurity content ($Z_{\mathrm{eff}} \sim 2$–2.5). The normalization is not important for the threshold identification but is essential to extract the correct intrinsic stiffness level χ_s. Far from threshold, q_i is theoretically foreseen to be linear with R/L_{Ti} [17]. In the range of q_i covered by the experiments, not too far from threshold, the experimental uncertainties do not allow to distinguish between linear and quadratic dependence. To allow comparison with previous work on electron stiffness, following the semiempirical critical-gradient model (CGM) described in [18], in the empirical modelling described below $f(R/L_{\mathrm{Ti}})$ was taken linear so that q_i is quadratic in R/L_{Ti}.

The experiment was performed in JET plasmas with $B_T = 3.36$ T, $I_p = 1.8$ MA, $q_{95} \sim 6$ (to minimize core sawtooth activity), $n_{e0} \sim 3$–4×10^{19} m^{-3}, $0.9 < T_e/T_i \sim 1.2$. The need to reach low values of q_i^{norm} to identify the threshold requires to minimize the centrally deposited power from Neutral Beam Injection (NBI). Therefore, the experiment was done in L-mode low rotating plasmas, retaining only the CX diagnostic NBI beam (1.5 MW). We also remark that the normalized curve holds the same whether in L- or H-mode, the latter being positioned closer to threshold due to higher temperatures. Most of heating was provided by ICRH (3–6 MW), using the multifrequency capability to vary between on- and off-axis ($\rho_{\mathrm{tor}} \sim 0.6$, where ρ_{tor} is the square root of the normalized toroidal magnetic flux). ICRH was applied in a (H)-D scheme (51 MHz on-axis, 42 MHz off-axis) with $n_H/n_e \sim 8\%$ and 30–60% of the ICRH core power delivered to thermal ions, and in a (^{3}He)-D scheme (33 MHz on-axis, 29 MHz off-axis) with $n_{3\mathrm{He}}/n_e \sim 5\%$ and 50–80% of the ICRH core power delivered to thermal ions. ICRH power deposition profiles have been calculated using the SELFO [19] code, while NBI power deposition was calculated by PENCIL [20]. The minority concentration was determined from the intensity of spectral lines [21] with an uncertainty of $\pm 2\%$, within which the ICRH ion power was found to vary by less than 12%. The analysis was carried out at the radial position $\rho_{\mathrm{tor}} = 0.33$ because it encloses the on-axis power but not the off-axis one, thus providing the maximum q_i scan. Values of R/L_{Ti} were calculated by an exponential best fit of T_i over 5 CX channels centered at $\rho_{\mathrm{tor}} = 0.33$ and averaged in time over a stationary interval. The gradient was taken with respect to the flux surface minor radius $\rho = (R_{\mathrm{out}}\text{-}R_{\mathrm{in}})/2$, where R_{out} and R_{in} are the outer and inner boundaries of the flux surface on the magnetic axis plane. The values of q_i were obtained by spatial integration of ion power density profiles and by determining the (small) collisional electron-ion transfer by means of interpretative transport simulations. The resulting q_i^{norm} vs R/L_{Ti} plot is shown in Fig. 1 (red circles). The points at neoclassical level were obtained by slowly modulating the NBI CX beam to measure just after switch on the T_i profile corresponding to zero NBI power. The gyro-Bohm normalization has been applied to q_i in two ways, to meet the inclinations of both theoreticians and experimentalists. The right Y scale indicates the values of q_i at $\rho_{\mathrm{tor}} = 0.33$ in gyro-Bohm units, i.e., q_i^{gB} [gB-units] $= q_i$ [MW/m^2]$/[(\rho_i/R)^2 v_{i\mathrm{th}} n_i T_i]$, where $v_{i\mathrm{th}} = \sqrt{T_i/m_i}$. The left Y scale indicates the total power in MW within $\rho_{\mathrm{tor}} = 0.33$ (which is proportional to q_i since all shots have the same geometry) and is normalized over $n_e T_i^{5/2}/R^2 B^2$ by rescaling the power to reference values of T_i (1.85 keV), n_e (3×10^{19} m^{-3}), B_T (3.36 T). The $q^{1.5}$ dependence was not included in the normalization because the local q has small variations across the data set ($q \sim 1.2$–1.5) and with large relative experimental uncertainties. Statistical error bars are not plotted for clarity's sake; they are typically $\Delta R/L_{\mathrm{Ti}} \sim \pm 0.3$–$0.6$ and $\Delta P_i^{\mathrm{norm}} \sim \pm 0.1$ MW. The threshold is well identified experimentally in Fig. 1 as the intercept at neoclassical heat flux, $R/L_{\mathrm{Ti\,crit}} = 3.5 \pm 0.3$. The ion stiffness appears to be high, as the excursion of

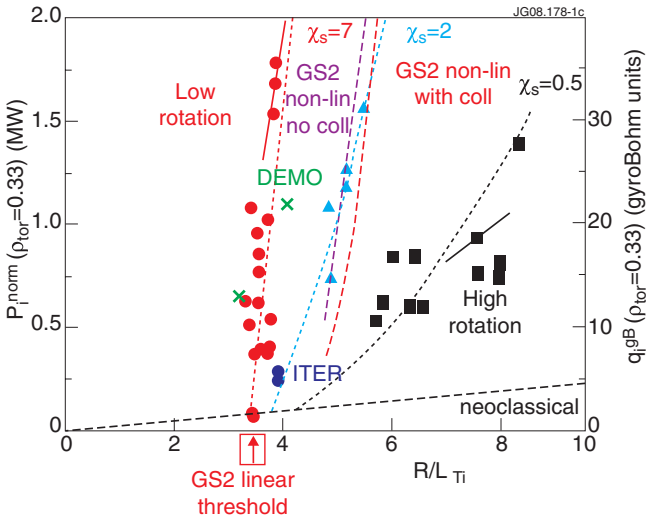

FIG. 1 (color online). Normalized q_i at $\rho_{\mathrm{tor}} = 0.33$ vs R/L_{Ti} for similar plasmas with different levels of rotation. Dots are experimental data and lines simulations. circles: $1 < \omega_{t0} < 2 \times 10^4$ rad/s, triangles: $3 < \omega_{t0} < 4 \times 10^4$ rad/s, squares: $5 < \omega_{t0} < 6 \times 10^4$ rad/s. The dashed black line is indicative of the neoclassical transport. The 2 segments indicate the local slope deduced from modulation. The 3 dotted lines are simulations using the CGM with different values of χ_s. The dashed thicker red and violet lines are nonlinear GS2 simulations with and without collisions, and the red arrow indicates the GS2 linear threshold for the low rotation shots. The ITER and DEMO positions (referring to right Y axis) are from simulations using the GLF23 model with two assumptions for the pedestal.

q_i^{norm} by over an order of magnitude does not lead to a significant change in R/L_{Ti}.

Blue triangles and black squares in Fig. 1 indicate high NBI power discharges with similar parameters but different levels of power and torque. Because of the gyro-Bohm normalization, they cover a similar range of q_i^{norm} as the low rotation shots. However, they show a significant increase of R/L_{Ti} with increasing rotation. In high rotation discharges, the threshold is obviously not identified due to lack of low q_i^{norm} points; therefore, the key question is whether the increase in R/L_{Ti} is due to an effect of rotational shearing rate ($\omega_{E\times B}$) on the threshold only, in accordance with theory predictions (i.e., keeping the same slope for all curves), or also on the stiffness level, as the data in Fig. 1 suggest. In the first case, one would need a shift in threshold $\Delta R/L_{\text{Ti}} \sim 4$, which is much larger than the value $\Delta R/L_{\text{Ti}} \sim 1$ predicted by the so-called "Waltz rule" [22]: $\gamma = \gamma_{\text{lin}} - \alpha_E \omega_{E\times B}$ with $\alpha_E \sim 0.6$ [23]. Such a high shift in threshold is very difficult to justify especially given the high stiffness measured in the low rotation shots. Assuming, instead, the validity of the Waltz rule for the shift in threshold, an upper limit for the change in the intrinsic stiffness coefficient χ_s has been estimated by fitting the data using the CGM [18]. The dotted lines in Fig. 1 indicate a change of χ_s from 7 to 0.5 with increasing rotation, leading to a factor 3 increase in R/L_{Ti} at similar values of the normalized heat flux. We attribute this variation to rotation because both its central value and its gradient change by a factor 6 over the dataset, while other parameters have only minor variations. Some variation is present in the ratio $R/L_{\text{Te}}/R/L_{\text{Ti}}$, ($\sim$1 in high rotation shots, $\sim$1.2–1.9 in low rotation shots). This is inherent in the fact that electrons are found less stiff than ions at low rotation, and the unavoidable fraction of ICRH electron power is sufficient to induce an increase of R/L_{Te} while R/L_{Ti} is kept at the threshold by the high ion stiffness. On the other hand, since the ion heat flux driven by R/L_{Te} is generally negligible [12], such variation should not affect our conclusions.

Since a more significant effect of rotation on stiffness than on threshold is a new observation, apparently not predicted by present theories, additional experimental evidence has been sought for confirmation. First of all, T_i modulation experiments in (^{3}He)-D have been performed both in low and high rotation plasmas to seek an independent confirmation of the factor 10 variation in slope observed in the steady-steady plot in Fig. 1. Three MW of ICRH on-axis power were square wave modulated at $\omega/2\pi = 6.25$ Hz and duty-cycle 70% for a total of 35 cycles. Figure 2 shows the amplitude (A) and phase (ϕ) profiles of the T_i perturbation at 6.25 and 12.5 Hz (and T_i profile in the insert) for two shots belonging to the red circle and black square sets in Fig. 1. It is immediately evident that the incremental diffusivity ($\chi_i^{\text{inc}} = -\partial q_i/n_i \partial \nabla T_i$), which is inversely proportional to the gradient of A and ϕ [10], is much lower in the high rotation shot. Normalizing by $T_i^{3/2}$ enhances the difference, as high rotation shots are also hotter. The two solid segments in Fig. 1 indicate the stiffness estimated from the modulation data using the simplified analytic formulae described in [10]. A more refined determination of χ_s was obtained with a time dependent transport simulation with the ASTRA code [24] using the CGM model [18]. The resulting A and ϕ profiles are also plotted in Fig. 2. The width and location of the ion deposition and the ion coupled power were taken from SELFO, while the time constant for the energy transfer from fast to thermal ions was adjusted in order to reproduce the measured ϕ absolute values. The contribution of

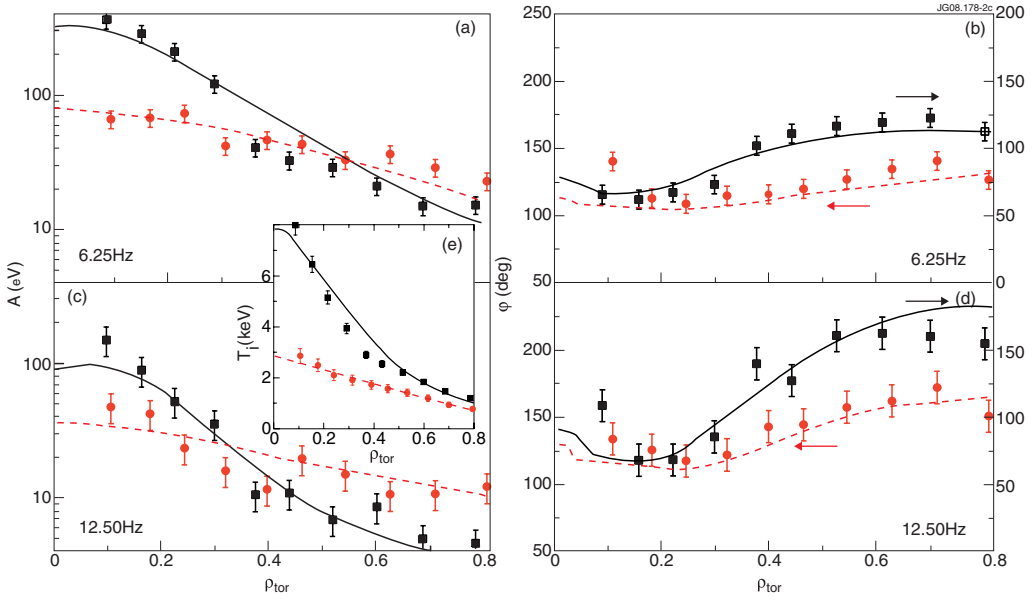

FIG. 2 (color online). Dots: experimental, lines: CGM-simulated profiles of T_i (e), A (a), (c) and ϕ (b), (d) at 2 modulation frequencies, for a low (73221, red circles) and a high rotation shot (73224, black squares).

the T_e modulation to the T_i modulation via collisional coupling is small and already accounted for since the simulation makes use of experimental T_e time traces, predicting only ions. Unlike in Fig. 1, which is local at $\rho_{\mathrm{tor}} = 0.33$, profiles of radially increasing threshold and stiffness had to be assumed to reproduce precisely the heat wave radial behavior in Fig. 2. The modulation and steady-state data can overall be satisfactorily fitted using at $\rho_{\mathrm{tor}} = 0.33$ $R/L_{\mathrm{Ti,crit}} = 3$, $\chi_s = 4$ at low rotation, and $R/L_{\mathrm{Ti,crit}} = 4$, $\chi_s = 0.2$ at high rotation. We conclude that the T_i modulation data directly confirm the factor 10 decrease in stiffness level seen at $\rho_{\mathrm{tor}} = 0.33$ in Fig. 1 with increasing rotation.

Second, the comparison of co- and counter-NBI plasmas with otherwise identical parameters (by reversing B_T and I_p in a dedicated campaign) shows that counter-NBI plasmas with very flat rotation profiles exhibit much lower R/L_{Ti} than co-NBI plasmas with peaked rotation. The comparison of ω_t and T_i profiles for a pair of co- and counter-NBI discharges is shown in Fig. 3. The flatter and lower toroidal rotation in the counter-NBI case is ascribed to off-axis torque deposition, also shown in Fig. 3(a) [25]. The non-normalized q_i is similar as shown in Fig. 3(b) (only 25% less ion heat flux in the counter-NBI case, which does not in itself justify the dramatic T_i decrease). Because of the lower T_i, the counter-NBI shot has a higher normalized heat flux; nevertheless, a dramatic reduction of R/L_{Ti} from 5.2 to 3.5 is observed [Fig. 3(b)]. In a q_i^{norm} vs R/L_{Ti} type of plot, the analysis of these pairs of co- and counter-NBI shots yields Fig. 4, which makes use of various times during the density ramp up leading to rotation decreasing in the counter-NBI case and remaining peaked in the co-NBI case. The final states of co- and counter-NBI shots (as shown in Fig. 3) indicate again a very important difference in stiffness level, while being compatible with a similar threshold. Lines in Fig. 4 are indicative of the CGM model stiffness levels compatible with the data.

Third, experiments in which NBI power is substituted with ICRH (H)-D power at constant total power have also been performed in JET H-mode plasmas [26]. The resulting q_i^{norm} vs R/L_{Ti} is plotted in Fig. 5, confirming the high stiffness in low rotation plasmas. However, from such data, only the small shift in threshold due to the increased rotational shear and lower T_e/T_i can be assessed. The smaller variation of q_i^{norm} in the NBI case (due to the broader NBI deposition and to the constraint of preserving power) prevents a conclusive demonstration of the decrease of stiffness. These experiments are therefore not suitable for a thorough assessment of the effect of rotation on transport.

Overall, we conclude that the available experimental evidence points consistently to a significant effect of rotation on ion stiffness in the inner half of the plasma in addition to a smaller effect on threshold.

The GS2 gyrokinetic code [27] has been used linearly and nonlinearly to address the experimental results at $\rho_{\mathrm{tor}} = 0.33$. The code does not include background $E \times B$ shear and thus cannot address effects of sheared plasma rotation and can only be compared to the low rotation data. Very good agreement is found between the linear GS2 threshold (indicated by the arrow in Fig. 1) and the value found in the experiment. The GS2 linear threshold has also been cross checked with the linear threshold by the GENE [28], GKW [29], and GYRO [30] gyrokinetic codes with very close match amongst the different codes. Minor variations were found in the linear threshold across all discharges in Fig. 1. The nonlinear GS2 predictions are drawn as dashed lines as indicated in Fig. 1, with and without ion-electron collisions. Adding also ion-ion collisions does not change the curve. Both curves yield a slope close to the experimental one, but an upshifted nonlinear threshold $R/L_{\mathrm{Ti}} \sim 4.5$–$4.8$, with a significant Dimits shift [17]. The experimental data however do not seem to support a significant upshift and are closer to the linear threshold. We conclude that nonlinear GS2 simulations are in agreement with ex-

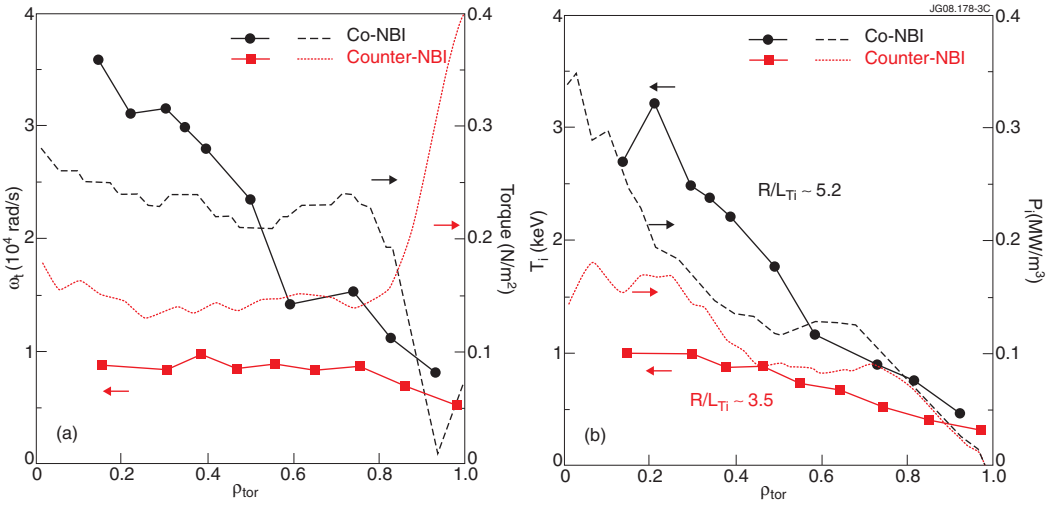

FIG. 3 (color online). Comparison of (a) absolute values of toroidal rotation and torque and (b) T_i and ICRH + NBI P_i profiles for a pair of similar JET discharges with co- (black circles and dashed lines) and counter-NBI (red squares and dotted lines).

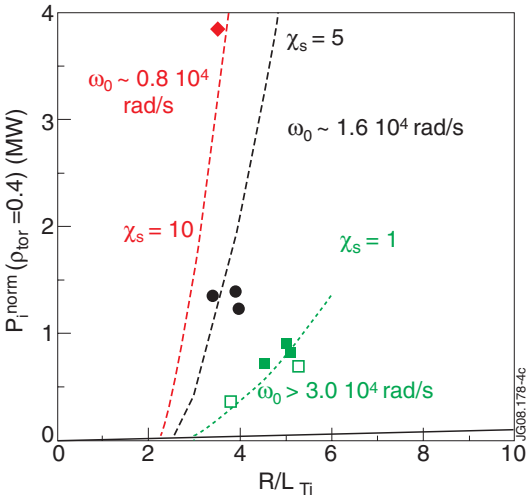

FIG. 4 (color online). P_i^{norm} at $\rho_{\mathrm{tor}} = 0.4$ vs R/L_{Ti} for co- (open symbols-58418) and counter-NBI (full symbols-59630, 59637) discharges. Different rotations are marked with different symbols/colors.

periment as far as ion stiffness is concerned, but overestimate the threshold due to the nonlinear upshift. The new result of a decrease in stiffness with increasing rotation requires novel theoretical investigation with codes including background $E \times B$ shear.

The implication of these findings is that rotation effects on stiffness cannot be ignored in addition to effects on threshold when interpreting experiments in present day machines aimed at identifying the role of rotation on confinement. Such results require careful, physics-based extrapolation to future devices. In fact, depending on how high above threshold in the normalized plot present experiments are performed and ITER or DEMO will operate (see their position in Fig. 1 based on GLF23 simulations), the

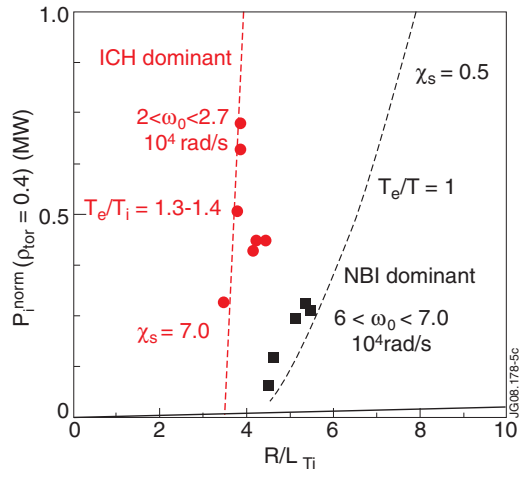

FIG. 5 (color online). P_i^{norm} at $\rho_{\mathrm{tor}} = 0.4$ vs R/L_{Ti} in a set of H-mode shots (50623-50630; 52092-52100) where NBI power (black squares) was substituted with ICRH power (red circles). The lines are the CGM model.

larger effect of rotation on stiffness may or may not dominate over the smaller effect on threshold.

We are grateful to C. Angioni, V. Naulin, and F. Ryter for stimulating discussions. We thank V. Parail and G. V. Pereverzev for providing ITER and DEMO simulations using GLF23. This work, supported by the European Communities under the contract of Association EURATOM/ ENEA-CNR, was carried out within the framework of EFDA. The views and opinions expressed herein do not necessarily reflect those of the European Commission. This work was done under the JET-EFDA workprogramme [31].

[1] R. C. Wolf *et al.*, Plasma Phys. Controlled Fusion **45**, 1757 (2003).
[2] A. G. Peeters *et al.*, Nucl. Fusion **42**, 1376 (2002).
[3] D. R. Baker *et al.*, Phys. Plasmas **8**, 4128 (2001).
[4] D. R. Baker *et al.*, Phys. Plasmas **10**, 4419 (2003).
[5] N. Mattor *et al.*, Phys. Fluids **31**, 1180 (1988).
[6] F. Romanelli *et al.*, Phys. Fluids B **1**, 1018 (1989).
[7] J. W. Connor and H. R. Wilson, Plasma Phys. Controlled Fusion **36**, 719 (1994).
[8] M. Kotschenreuther *et al.*, Phys. Plasmas **2**, 2381 (1995).
[9] G. Tardini *et al.*, Nucl. Fusion **42**, 258 (2002).
[10] P. Mantica and F. Ryter, C.R. Physique **7**, 634 (2006).
[11] D. R. Mikkelsen *et al.*, Nucl. Fusion **43**, 30 (2003).
[12] F. Ryter *et al.*, in *Proceedings of the 22nd Int. Conf. on Fusion Energy, Geneva 2008* (International Atomic Energy Agency (IAEA), Vienna, 2008), EX/P5-19.
[13] F. Ryter *et al.*, Phys. Rev. Lett. **95**, 085001 (2005).
[14] F. Ryter *et al.*, Plasma Phys. Controlled Fusion **48**, B453 (2006).
[15] A. G. Peeters *et al.*, Phys. Plasmas **12**, 022505 (2005).
[16] X. Garbet *et al.*, Plasma Phys. Controlled Fusion **46**, B557 (2004).
[17] A. M. Dimits *et al.*, Phys. Plasmas **7**, 969 (2000).
[18] X. Garbet *et al.*, Plasma Phys. Controlled Fusion **46**, 1351 (2004).
[19] J. Hedin *et al.*, Nucl. Fusion **42**, 527 (2002).
[20] C. D. Challis *et al.*, Nucl. Fusion **29**, 563 (1989).
[21] D. Van Eester *et al.*, Plasma Phys. Controlled Fusion **51**, 044007 (2009).
[22] R. E. Waltz *et al.*, Phys. Plasmas **1**, 2229 (1994).
[23] J. Kinsey *et al.*, Phys. Plasmas **14**, 102306 (2007).
[24] G. V. Pereverzev *et al.*, Max-Planck Report, IPP 5/98, 2002.
[25] P. De Vries *et al.*, Nucl. Fusion **48**, 065006 (2008).
[26] W. Suttrop *et al.*, Europhys. Conf. Abstr. A **25**, 989 (2001).
[27] M. Kotschenreuther *et al.*, Comput. Phys. Commun. **88**, 128 (1995).
[28] F. Jenko *et al.*, Phys. Plasmas **7**, 1904 (2000).
[29] A. G. Peeters *et al.*, Phys. Plasmas **11**, 3748 (2004).
[30] J. Candy and R. E. Waltz, J. Comput. Phys. **186**, 545 (2003).
[31] F. Romanelli *et al.*, *Proceedings of the 22nd Int. Conf. on Fusion Energy, Geneva, 2008* [International Atomic Energy Agency (IAEA), Vienna, 2008]. (All the members of the JET-EFDA collaboration appear in the appendix of this paper.)